

Research article

Re-assembled Casein Micelles for Oral Delivery of Chemotherapeutic Combinations to Overcome Multidrug Resistance in Gastric Cancer

Maya Bar-Zeev^{1,2,3}, Lotem Nativ^{1,4}, Yehuda G. Assaraf^{3*}, Yoav D. Livney^{1,2*}¹The Laboratory of Food Physical Chemistry and Biopolymeric Delivery Systems for Health, Department of Biotechnology and Food Engineering, Technion - Israel Institute of Technology, Haifa 3200000, Israel²Russell Berrie Nanotechnology Institute, Technion - Israel Institute of Technology, Haifa 3200000, Israel³The Fred Wyszowski Cancer Research Laboratory, Department of Biology, Technion - Israel Institute of Technology, Haifa 3200000, Israel⁴Current address: Department of Psychology and Brain Sciences, University of Massachusetts Amherst, MA, 01003, USA

*Correspondence: livney@technion.ac.il (Yoav D. Livney)

<https://doi.org/10.31083/j.jmcm.2018.01.008>**Abstract**

Multidrug resistance (MDR) mediated by ATP-dependent efflux transporters continues to be a dominant obstacle towards curative cancer therapy. We have previously demonstrated the ability of β -casein micelles (β -CM) to orally deliver a combination of individually encapsulated hydrophobic cargo of drugs and chemosensitizers designed to overcome MDR in gastric cancer. Herein we investigated the potential of re-assembled casein micelles (rCM) to serve as a target-activated delivery platform comprising a synergistic duo of a chemotherapeutic drug (paclitaxel) and a P-glycoprotein-specific transport inhibitor (tariquidar). The high binding affinity of paclitaxel and tariquidar to rCM was demonstrated by spectrofluorometry. Furthermore, solubilization of the drugs and suppression of crystal growth was shown by light microscopy and dynamic light scattering. A remarkable anti-tumor activity and complete MDR reversal were demonstrated in the *in vitro* cytotoxicity assay against MDR human gastric carcinoma cells overexpressing P-glycoprotein. The structure and cytotoxic activity of drug-loaded rCM were completely retained after freeze-drying and reconstitution as in β -CM. Hence, our findings highlight the great potential of casein-based nanovehicles as efficient platforms for oral delivery and local target-activated release of synergistic hydrophobic drug combinations to treat gastric cancer, and overcome of cancer chemoresistance, and for the possible treatment of non-malignant gastric disorders.

Keywords

Re-assembled-casein micelles; Target-activated oral delivery; Gastric cancer; Chemotherapeutics; Paclitaxel; Multidrug resistance; Efflux pumps; Chemosensitizers; Tariquidar

Submitted: November 22, 2017; Accepted: December 3, 2017

1. Introduction

Cancer remains one of the leading causes of death worldwide. In recent years there has been much progress in the treatment of various cancers. However, the prognosis of diverse carcinomas remains dismal including that of gastric cancer [1]. A dominant impediment towards curative cancer therapy is multidrug resistance (MDR) [2–4], a spectrum of inherent (i.e. existing prior to chemotherapeutic drug treatment) or *de novo* acquired (i.e., following anticancer drug treatment) mechanisms that mediate cancer cell resistance to multiple structurally and mechanistically distinct cytotoxic drugs [5–8]. The most common mechanism of MDR is enhanced energy-dependent efflux of various hydrophobic cytotoxic drugs, which diffuse into cells through the plasma membrane [9]. This ATP-driven efflux of chemo-therapeutics from the cell is mediated by transmembrane transporters of the ATP-binding cassette (ABC) superfamily [9–11]. P-glycoprotein (P-gp; ABCB1; MDR1), which is overexpressed in various cancers, is considered to be one of the three dominant efflux pumps that diminish the efficacy of numerous hydrophobic chemotherapeutics [2]. MDR modulators, also known as chemosensitizers, achieve MDR reversal and re-sensitization of MDR can-

cer cells to chemotherapy by blocking specific MDR efflux transporters [12, 13].

Bovine milk is comprised of ~80% phosphoproteins known as Caseins. Their amphiphilic structure enables 80–95% of them to naturally self-assemble into casein (CN) micelles (CM), which are spherical particles, ranging from 50 to 500 nm in diameter (average 150 nm) [14–16]. CM are composed of four caseins: α_{s1} -, α_{s2} -, β - and κ -CN supported by calcium-phosphate nanocluster bridging to serine-phosphate residues of α_{s1} -, α_{s2} - and β -caseins, and by hydrophobic interactions [15, 17]. CM naturally function as a nano-delivery system, transporting essential nutrients, primarily calcium, phosphate and protein, from the mother to the neonate [14, 16]. The open structure of caseins, resulting from their proline-rich sequence, facilitates high accessibility to gastric proteolytic enzymes. This structure provides target-activated release, of the cargo, loaded in the CM, in the stomach [15, 16]. Reconstitution of the mineral composition of milk can produce re-assembled CM (rCM) *in vitro* from soluble caseinate [14, 16]. Another advantage of rCM stems from the natural gelling mechanism of CM at low pH, near the isoelectric pH of the caseins (~4.6). This mechanism has evolved

to provide sustained release of peptides following milk ingestion by the baby. In a series of studies, we have demonstrated that rCM, as well as individual caseins (e.g., β -CN), can be harnessed to serve as nanovehicles for oral delivery of hydrophobic cargo including nutraceuticals [14, 16, 18–20] and chemotherapeutic agents [21–25]. As we have previously described [25], drug entrapment in a gastrically-digestible protein is expected to reduce the adverse toxicity of chemotherapeutics to the buccal cavity and esophagus, and provide a locally focused treatment due to the depletion of the gastric mucosa lining in the tumor surrounding [26]. Hence, rCM could be used as an oral delivery nanovehicle for the target-activated release of chemotherapeutic drugs in the stomach, thereby minimizing toxic side effects caused by systemic chemotherapy.

Chemotherapeutic drugs possess various characteristics (e.g., high lipophilicity and poor water solubility) limiting their oral bioavailability. A suitable and effective oral drug administration form will drastically improve the quality of life of cancer patients and will significantly reduce the treatment cost by reducing unnecessary hospitalizations, which put the patients at a life-threatening risk due to antibiotic-resistant bacteria prevalent in hospitals [27, 28]. Anticancer nanomedicine is a promising therapeutic approach that could overcome various limitations of conventional small-molecule chemotherapeutics. Nanovehicles enable solubilization of hydrophobic drugs, delivery of various drug combinations and programmable targeted drug release at the tumor site [2–4]. These advantages can also be harnessed to overcome cancer MDR.

The current study focused on developing CM, in particular rCM, as oral delivery nanovehicles of synergistic combinations of hydrophobic chemotherapeutic drugs and MDR modulators for the treatment of MDR gastric cancer. In the current study constitutes the first examination this delivery platform (rCM), loaded with chemotherapeutic drugs, based on the hypothesis that due to the evolutionary ability of CM to be easily digested in the stomach, one will obtain a target-activated release for local gastric treatment. Moreover, chemosensitizers should enhance the bioavailability of the chemotherapeutic drugs in MDR cancer cells. Therefore, this natural delivery system is expected to display a synergistic effect in overcoming MDR in gastric cancer. The objectives of the current research were to individually load rCM with a chemotherapeutic drug (paclitaxel (PTX)) and a potent chemosensitizer (tariquidar (TQD)); to characterize the micelles formed and to evaluate the efficacy of this combined system against human P-gp-dependent MDR gastric cancer cells, before and after freeze-drying and reconstitution, and to compare rCM and β -CM as nanovehicles for oral anti-cancer target-activated drug delivery.

2. Materials and methods

2.1. Preparation of drug-loaded rCM and β -CM

Sodium caseinate (Casinella-QN, 94.2% protein) was a kind gift from Kelta Ltd, Israel, and Molkerei Meggle Wasserburg GmbH & Co. KG, Germany. β -CN (Lot number: JC2-013-05, total protein 88%, of which 76% is β -CN) was generously provided by ARLA (ARLA Food Ingredients, Viby, Denmark) and was further purified as previously described [29]. Potassium phosphate dibasic, potassium citrate tribasic monohydrate, calcium chloride dihydrate, paclitaxel (T7191) and daunorubicin (D8809) were purchased from Sigma-Aldrich (Rehovot, Israel). Tariquidar was purchased from MedKoo Bioscience (Chapel Hill, NC, USA).

2.2. Simulated digestion

Pepsin (P7000; ≥ 250 units/mg protein), trypsin (T0303; 13,000–20,000 BAEE [N α -benzoyl-L-arginine ethyl ester as substrate] units/mg protein), chymotrypsin (C4129; ≥ 40 units/mg protein), pancreatic lipase (L3126; 100–500 units/mg protein), sodium glycodeoxycholate (G9910) and taurocholic acid sodium salt hydrate (T4009) were obtained from Sigma-Aldrich (Rehovot, Israel). Sodium chloride and sodium bicarbonate were obtained from Frutarom Industries Ltd. (Haifa, Israel) and hydrochloric acid was purchased from Gadot Group (Netanya, Israel).

2.3. Tissue culture

Leibovitz L-15 medium, fetuin, transferrin and D-glucose were purchased from Sigma-Aldrich (Rehovot, Israel). Fetal calf serum, minimal essential vitamins, glutamine, insulin, penicillin and streptomycin were purchased from Biological Industries (Beit-HaEmek, Israel).

2.4. Preparation of drug-loaded re-assembled casein micelles (drug-rCM), freeze-drying and reconstitution

2.4.1. Preparation of drug-loaded rCM

Drug-loaded rCM were prepared based on the protocol we previously described [16, 20]. Briefly, sodium caseinate was dissolved in double distilled water (DDW) by an overnight stirring at room temperature to obtain full hydration. Drug loading at varying drug:CN molar ratios (CN molecular mass used for calculations was 24 kDa) was achieved by adding different volumes of the drug solution in DMSO to the 2% sodium caseinate solution, followed by 30 min stirring. Thereafter, 0.08 M K_2HPO_4 and 0.4 M tri-potassium citrate solutions were added, followed by dropwise addition of 0.03 M $CaCl_2$ solution while mixing. A control of rCM without the drugs were prepared similarly, except that an equivalent amount of pure DMSO was added to the sodium caseinate solution instead of the drug solutions. The final volume percentage of DMSO in the samples did not exceed 1.7%.

2.4.2. Drug encapsulation in β -CM

Drug entrapment in β -CM was performed as we previously described [21, 25]. β -CN concentration in all samples was above the critical micellization concentration of pure β -CN [30]. The volume percentage of DMSO in PBS did not exceed 1.0%.

2.4.3. Freeze-drying and reconstitution

Before freeze-drying, maltodextrin, a cryoprotectant, as added to the rCM solutions at a 5% (wt/wt) concentration, followed by stirring for 1 hr at room temperature. All samples (rCM and β -CM) were quench-frozen in liquid nitrogen, freeze-dried and then reconstituted. Reconstitution was performed by adding DDW. Following the addition of DDW, rCM were stirred overnight at 4°C and β -CM were stirred for 1 hr at room temperature.

2.5. Evaluation of the interaction and solubilization by visual observation

Samples of pure PTX (417 μ M), TQD (250 μ M) and of the respective drug at the same concentration loaded into rCM (1 mg/ml rCM, at 10:1 and 6:1 drug:CN molar ratios, respectively) were pre-

pared containing a final DMSO concentration of 1.0% (v/v). Photographs were taken using a digital SLR camera, Nikon D700, with a Tamaron AF 28–75 mm f/2.8 XR Di LD lens. A representative image was chosen following two independent experiments.

2.6. Binding studies by fluorescence spectroscopy

Binding affinities of PTX and TQD to rCM were determined by fluorescence quenching of the intrinsic tryptophan (Trp) fluorescence of CN. Trp fluorescence was determined by excitation at 280 nm and recording the emission spectra from 290 to 450 nm, with 5 nm slit widths, using Cary Eclipse fluorescence spectrophotometer (Agilent Technologies). CN fluorescence was monitored at a constant protein concentration of 1 mg/ml and either PTX or TQD at increasing drug:CN molar ratios. Samples contained 1.0% (v/v) DMSO. Measurements were performed in triplicates at 23°C, and the average value and standard error (SE) were calculated. Association constant calculations were done using the Langmuir based model [31–33], as described by Equation (1):

$$F_0 - F = \frac{(F_0 - F_\infty)L_0}{1/K_a + L_0} \quad (1)$$

Where F and F_0 are rCM fluorescence intensity in the presence and absence of the drug, respectively; F_∞ is the fluorescence when the protein micelles are saturated, $[L_0]$ is the drug concentration and K_a is the association constant. Statistical analysis and nonlinear curve fitting were performed using the OriginPro 9.0 software (OriginLab Corporation, Northampton, MA, USA).

2.7. Particles size distribution by dynamic light scattering (DLS)

Particle size distributions of drug-loaded CM (without calcium and phosphate) at various drug:CN molar ratios were studied using a DLS analyzer, NICOMP™ 380 (Particle Sizing System (PSS), Inc., Santa Barbara, CA, USA). The laser wavelength was 658 nm. The Avalanche photodiode detector for scattered light intensity was at a fixed angle of 90°. Scattered light intensity fluctuation measurements were analyzed by the NICOMP™ volume-weighted particle size distribution analysis [22]. The size range for the NICOMP™ distribution analysis was set to 1–1000 nm. Samples contained up to 1.0% (v/v) DMSO. Measurements were made in triplicates at 23°C, and mean values and SE were calculated. Identical operation parameters were used to determine particle size distributions of drug loaded rCM before and after freeze-drying and reconstitution.

2.8. Evaluation of binding stoichiometry by light microscopy

Binding stoichiometry and crystal formation of drug-loaded rCM compared to the free drugs were studied using light microscopy. Olympus BX51 light microscope was operated in Nomarski differential interference contrast (DIC) and polarized light optical modes ($\times 40$ magnification, 24°C). Pictures were acquired using an Olympus DP71 digital camera connected to the microscope. Samples of 417 and 500 μM pure PTX, 250 and 333 μM pure TQD, as well as rCM with each of these drugs at the same concentration (molar ratio of drug:CN, respectively: 10:1, 12:1 6:1, and 8:1), were examined. Samples contained a final DMSO concentration of 1.0% (v/v). Approximately 10 similar images of each of the samples were collected in two independent experiments.

2.9. In vitro simulated digestion

2.9.1. Simulated digestion model

To evaluate rCM digestibility and the drug release profiles, a standardized static *in vitro* digestion protocol was used [34]. The simulated digestion was comprised of two parts: a 1 hr simulated gastric digestion (SGD) followed by a 2 hr simulated intestinal digestion. Samples were taken after 5, 10, 20, 30 and 60 min during the gastric phase as well as after 5, 60 and 120 min of the intestinal digestion phase. To terminate the enzymatic activity Pefablock® SC (Roche) was added and samples were quench-frozen using liquid nitrogen.

2.9.2. Monitoring protein degradation during simulated gastrointestinal digestion

Proteolytic casein degradation as a function of simulated digestion time was examined using a sodium dodecyl sulfate-polyacrylamide gel (15% acrylamide; SDS-PAGE) electrophoresis. Protein samples (10 μg) from the simulated digestion were loaded and resultant protein bands were stained with Coomassie brilliant blue. A typical gel demonstrating the gastrointestinal digestion profile observed for the three systems tested (rCM, 6:1 molar ratio of PTX:CN and 4:1 molar ratio of TQD:CN) is presented.

2.10. Cytotoxicity assays

2.10.1. Tissue culture

Human parental gastric carcinoma cells, EPG85-257P, and their MDR subline overexpressing P-gp, EPG85-257RDB, were generously provided by Prof. H. Lage (Charité - Medicine University, Berlin, Germany). Cells were cultured as previously described [25] in Leibovitz L-15 medium, supplemented with 10% fetal calf serum, 1 mM glutamine, 6.25 mg/l fetuin, 80 IE/l insulin, 2.5 mg/l transferrin, 0.5 g/l D-glucose, 1.12 g/l NaHCO₃, 1% minimal essential vitamins, 100 $\mu\text{g}/\text{ml}$ penicillin and 100 units/ml streptomycin. Cells were grown in a humidified atmosphere of 5% CO₂ and at 37°C. The growth medium of the MDR subline was additionally supplemented with 4.4 μM daunorubicin. MDR cells were cultured in a drug-free medium for a week before each experiment.

2.10.2. Cytotoxicity assays

Cells were seeded at 3×10^3 cells/well in 96-well plates (100 $\mu\text{l}/\text{well}$). After a 24 hr incubation, cells were exposed to the different systems at increasing PTX concentrations (up to 0.1% (v/v) DMSO) for 1 hr (simulating the average residence time in the stomach of 0.5–4 hr after food ingestion [35]). This drug exposure was followed by three washes with complete growth medium or PBS (for the undigested systems) in order to remove the excess drug. After additional 48 hr of incubation, cell viability was determined using a colorimetric XTT-based cell proliferation assay (Biological Industries, Beit-HaEmek, Israel).

PTX cytotoxicity in the presence and absence of 0.8 μM TQD was determined using solutions of the free drugs in DMSO, and solutions of the drugs released by SGD, diluted in complete growth medium. The cytotoxicity of the undigested drugs loaded in rCM was studied in a serum-free medium (SFM) due to the previously described [24] competitive binding of the hydrophobic drugs to serum albumin, which is not present in the stomach. The rCM-based

delivery system is designed for oral delivery, therefore, the rCM will not be exposed to direct contact with serum albumin.

Cytotoxicity data were analyzed with OriginPro 9.0 using a nonlinear curve fitting for dose-response curve according to Equation (2) [24]:

$$P = P_{\infty} + (P_0 - P_{\infty}) \left(\frac{[D]^n}{IC_{50}^n + [D]^n} \right)$$

Where P represents the percentage of surviving cells at each drug concentration, P_0 represents the maximal percent of live cells (absence of drug, 100% = control), P_{∞} denotes the minimal percentage of surviving cells (infinite drug concentration, maximal response is characterized by 0% viability of cells), $[D]$ represents the drug concentration, IC_{50} is the drug concentration exerting 50% inhibition of cell growth and n is the Hill slope parameter for the dose-response curve. Results shown are means \pm SE obtained from three independent experiments, each performed in triplicates. The statistical

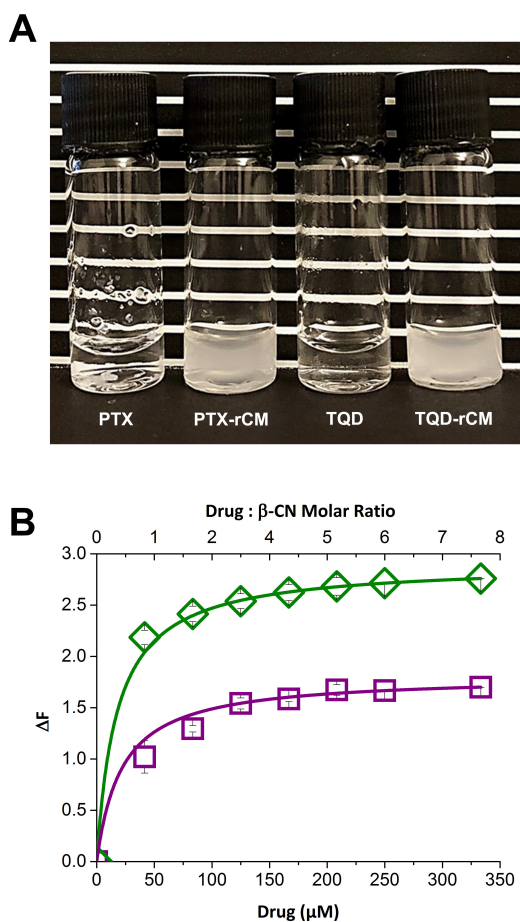


Fig. 1. Drug-CN binding studies. (A) Photographs of 417 μM pure PTX (left pair of vials) and 250 μM TQD (right pair of vials) in DDW (left vials in each pair) vs. each of the drugs, at the same concentration, in 1 mg/ml sodium caseinate (right vials in each pair; 10:1 and 6:1 drug: CN molar ratio, respectively). (B) Fluorescence quenching of CN by PTX (\square) and TQD (\diamond) as a function of drug: CN molar ratio (top axis) and drug concentration (bottom axis). Excitation: 280 nm and Emission: 350 nm. The curve represents a Langmuir-based adsorption model described in Equation (1); error bars represent SE. K_d (PTX) = $0.46 \times 10^5 \pm 0.41 M^{-1}$; K_d (TQD) = $0.57 \times 10^5 \pm 0.07 M^{-1}$.

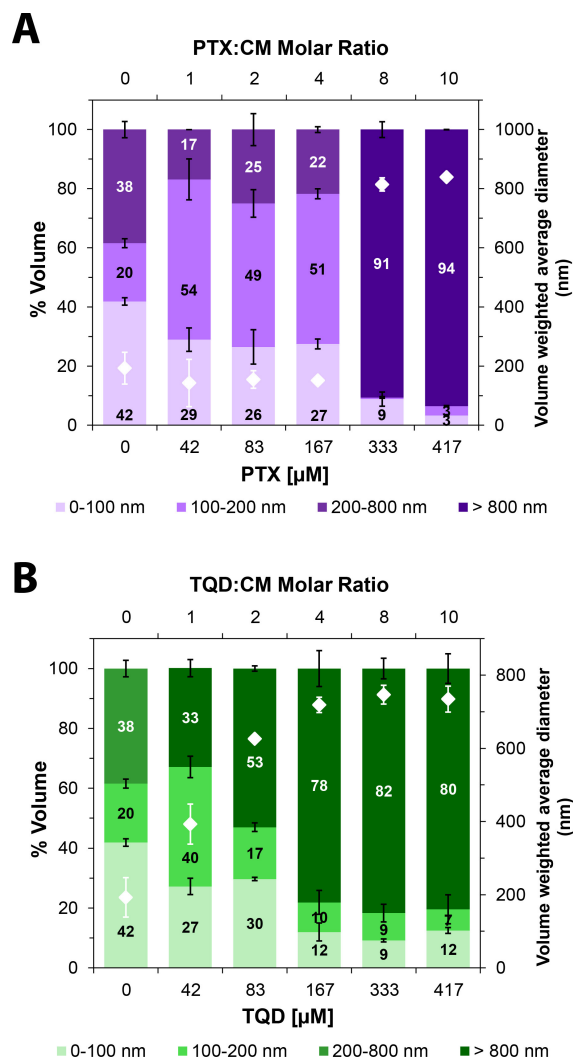


Fig. 2. Nanoparticle size distribution. Volume-weighted percent of (A) PTX and (B) TQD in 1 mg/ml rCM and overall average diameter (\diamond) as a function of the molar ratio of drug: CN (top axis) and drug concentration (bottom axis); error bars represent SE.

analysis of variance of the calculated IC_{50} values was determined using an unpaired student's T-test. A P -value lower than 0.05 was considered statistically significant.

3. Results

3.1. Drug-rCM binding studies

In Fig. 1A, the photographs of the pure drugs in DDW versus an equivalent concentration of drug-loaded rCM demonstrate that drug binding to rCM has occurred. The free drugs, PTX and TQD, precipitated and formed visible aggregates. In contrast, when these drugs were loaded into rCM at the same concentrations, they were entrapped within the protein micelles, and underwent solubilization, resulting in a sediment-free, uniform nano-dispersion. These findings visually suggest that casein binds PTX and TQD. To further substantiate this finding, we used quenching of the intrinsic tryptophan fluorescence of CN to quantify drug binding to CN. Fig. 1B shows the quenching of CN fluorescence by each of the loaded drugs

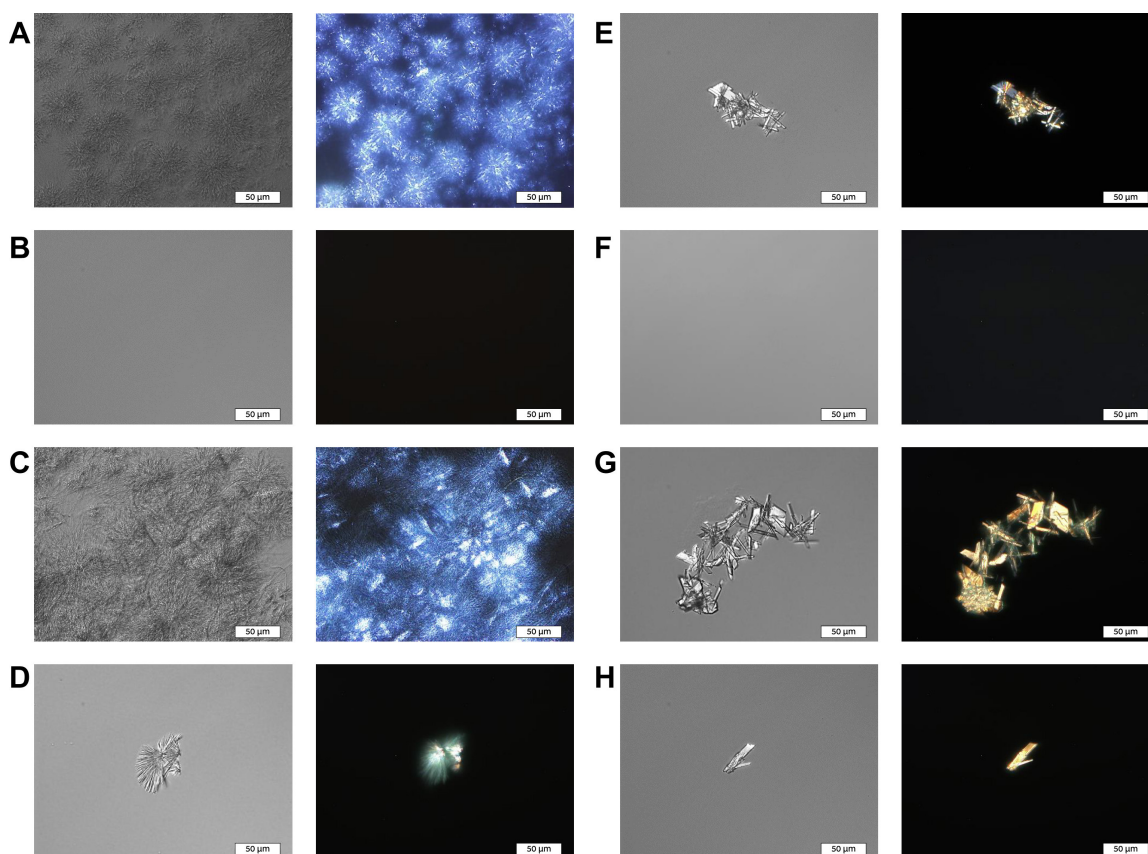


Fig. 3. Drug-CN binding stoichiometry and visualization of crystallization. Nomarski DIC (left) and polarized light microscopy (right) images (x40 magnification) of: (A) 417 μM , (C) 500 μM pure PTX in DDW vs. (B) 417 μM , (D) 500 μM PTX in 1 mg/ml rCM (10:1, 12:1 drug: CN molar ratio, respectively) and (E) 250 μM , (G) 333 μM pure TQD in PBS vs. (F) 250 μM , (H) 333 μM TQD in 1 mg/ml rCM (6:1, 8:1 drug: CN molar ratios, respectively). Scale bar: 50 μm .

as a function of the drug:CN molar ratio. These results confirmed the existence of binding-induced static quenching. Upon excitation at 280 nm, the emission intensity at 350 nm was recorded; the association constants (K_a) values were calculated from the non-linear curve fit of the Langmuir-based adsorption model [31–33] (Equation (1)). The results indicate that both PTX and TQD bind to CN. The association constants of PTX-CN and TQD-CN were found to be $4.61 \times 10^4 \pm 0.41 \text{ M}^{-1}$ and $5.68 \times 10^4 \pm 0.07 \text{ M}^{-1}$, respectively, with R^2 value of 0.99. Thus, CN exhibits a similar affinity towards both PTX and TQD.

3.2. Nanoparticle size distribution

Size distribution of rCM loaded with PTX or TQD, at increasing drug: CN molar ratios, was evaluated by DLS. Fig. 2 shows that particle size distribution is directly affected by the drug:CN molar ratio as we previously reported for drug-loaded β -CN micelles [21, 23–25]. At low PTX concentrations, more than 70% of the particles were smaller than 200 nm. Upon increasing drug concentrations (increased drug:CN molar ratio), PTX appears to initially bind to the caseins and is entrapped within the hydrophobic core of the micelles until they are maximally loaded. At higher molar ratios, the excess drug starts forming increasingly larger microcrystals, which become visible above a few microns under polarized light (Fig. 3). TQD-rCM display a similar structural organization comprising TQD-

rCM incorporating nano-sized TQD crystals at a lower drug:CN molar ratios, exerting a slightly lower maximal loading capacity. These findings demonstrate that the rCM-mediated entrapment and stabilization of PTX and TQD against crystallization and aggregation. To determine the maximal loading capacity, we used polarized light microscopy and sought the maximal drug concentration beyond which visible microcrystals appear (Fig. 3).

3.3. Evaluation of drug-rCM binding stoichiometry

Fig. 3 shows a comparison between light microscopy images of the free drugs in DDW (A, C, E and G) and the same drug concentrations loaded into rCM (B, D, F and H, respectively). Figs 3A, C, E and G, confirm that the drug concentrations were above their solubility limit in aqueous solution, which caused micro-sized crystal formation. Conversely, in Figs 3B, D, F and H, the drug-loaded r-CM demonstrated sub-micron-sized particles. As we previously described for β -CN-based micelles [21, 23–25], rCM also appear to suppress drug crystal growth and aggregation [29, 36] by efficient drug binding and encapsulation. The maximal loading capacity of PTX, according to the light microscope was observed at 10:1 PTX:CN molar ratio (B), above which, at a molar ratio of 12:1 PTX:CN, PTX crystals were observed (D). In a similar manner, for TQD, the maximal loading capacity observed was lower and was found to be 6:1 TQD:CN molar ratio (F). Examination of a higher

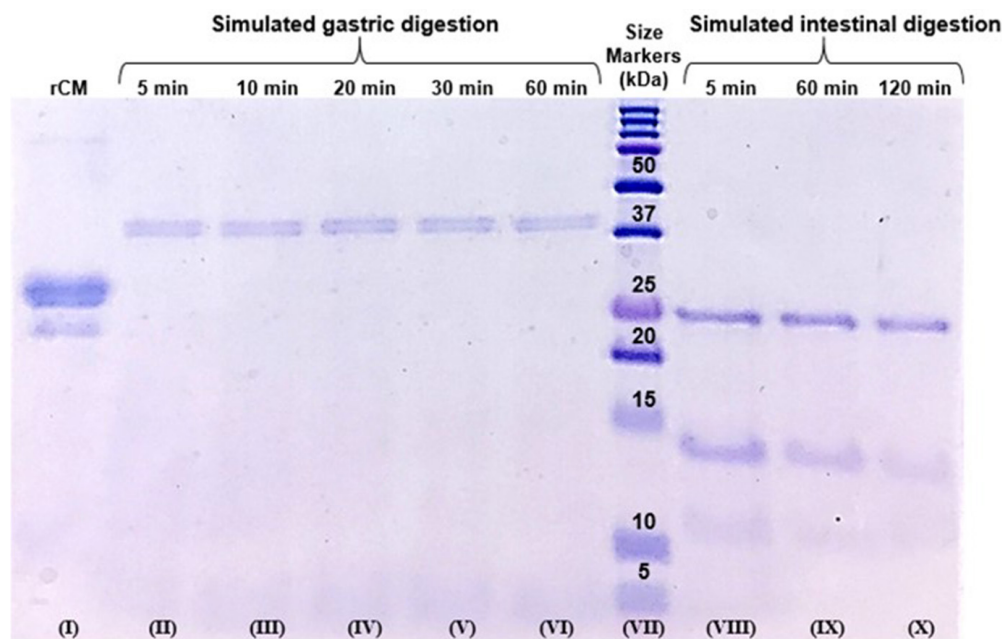


Fig. 4. Proteolytic degradation of rCM during simulated gastrointestinal digestion. SDS-PAGE analysis of rCM degradation products in a simulated gastrointestinal digestion process as a function of the two-phase digestion times. Lanes: (I) rCM before the simulated digestion, simulated gastric digestion for various times: (II) 5 min, (III) 10 min, (IV) 20 min, (V) 30 min, (VI) 60 min, (VII) size markers (top to bottom): 250, 150, 100, 75, 50, 37, 25, 20, 15, 10 and 5 kDa, simulated intestinal digestion time: (VIII) 5 min, (IX) 60 min, and (X) 120 min.

molar ratio of 8:1 TQD:CN, resulted in a super-saturation causing crystal formation (H).

3.4. Protein degradation by *in vitro* simulated digestion

Casein digestibility, and drug release rates in the stomach, were evaluated using a standardized static *in vitro* gastrointestinal digestion model [34] on rCM samples and drug-loaded rCM samples. Fig. 4 depicts the proteolysis pattern of rCM as a function of digestion time as revealed by SDS-PAGE (a representative SDS PAGE gel is shown). The protein composition prior to the proteolytic digestion is presented in lane (I). The molecular masses of the four caseins, α_{s1} -, α_{s2} -, β - and κ -casein in bovine milk are 23, 25, 24 and 19 kDa, respectively [15], and are seen in lane (I), although not fully resolved, due to the close molecular masses of α_{s1} -, α_{s2} - and β -CN. Lanes (II)-(VI) depict rCM degradation under SGD conditions after 5, 10, 20, 30 and 60 min of incubation at 37°C, respectively. In these lanes, the levels of the two bands representing the four caseins diminished and a band of ~37 kDa in size was observed, which is attributable to the pepsin (the molecular mass of pepsin is 35 kDa). Lanes (VIII)-(X) show a simulated intestinal digestion for 5, 60 and 120 min, respectively. Bands of ~25 kDa appeared in these lanes. These bands are attributable to the chymotrypsin (molecular mass of 25 kDa) and trypsin (molecular mass of 23.5 kDa) that were added in the intestinal digestion stage. Our results regarding the rate of the gastrointestinal breakdown of the caseins are in line with our previous studies [15, 20, 24] and with the literature [37, 38]. To test the influence of loaded PTX or TQD on the digestibility of rCM, both PTX-rCM and TQD-rCM (6:1 and 4:1 drug:CN molar ratio, respectively) breakdown during simulated digestion was studied using SDS-PAGE. Extremely similar SDS-PAGE results were obtained for both systems tested (data not shown) in comparison with drug-

free rCM, demonstrating that the presence of these drugs had no significant influence on the kinetics of the gastrointestinal proteolytic digestion process.

3.5. Cytotoxic activity of drug-loaded rCM

The cytotoxic activity of free PTX was compared with that of PTX-rCM (6:1 PTX:CN molar ratio, before and after SGD) with or without the addition of the potent P-gp transport inhibitor TQD, either free or loaded onto rCM (4:1 TQD:CN molar ratio, before and after SGD). The percentage of surviving cells vs. PTX concentration is presented in Fig. 5A-C and the IC₅₀ values derived from the sigmoidal fitting of the dose-response curves using Equation (2), are depicted in Fig. 5D.

Control samples of digested rCM and 0.1% DMSO (v/v) in complete growth medium (Fig. 5E) and undigested rCM and 0.1% DMSO (v/v) in SFM (Fig. 5F) were tested by a 1 hr pulse exposure of the cells. No cytotoxic activity was observed with these drug-free controls. In contrast, the P-gp-overexpressing MDR subline EPG85-257RDB exhibited a 113-fold resistance to free PTX (Fig. 5A, D) compared to their parental cells EPG85-257P which are devoid of P-gp expression. The mean IC₅₀ values obtained for wild type EPG85-257P cells and their MDR subline EPG85-257RDB were 23.7 ± 3.3 and $2,688 \pm 794$ nM, respectively. Addition of 0.8 μ M free TQD completely reversed this resistance. Similarly, EPG85-257RDB cells displayed 130-fold resistance to PTX-rCM following SGD. These results provide evidence that the cytotoxic activity of PTX and TQD was not compromised due to the gastric digestion, since the IC₅₀ values for the digested drug-loaded rCM (in both parental and MDR cell lines: 27.5 ± 2.4 nM and $3,563 \pm 607$ nM, respectively; Fig. 5B, D) were not significantly different ($P = 0.4105$ and $P = 0.4017$, respectively) from those of the undigested free PTX (Fig. 5A, D).

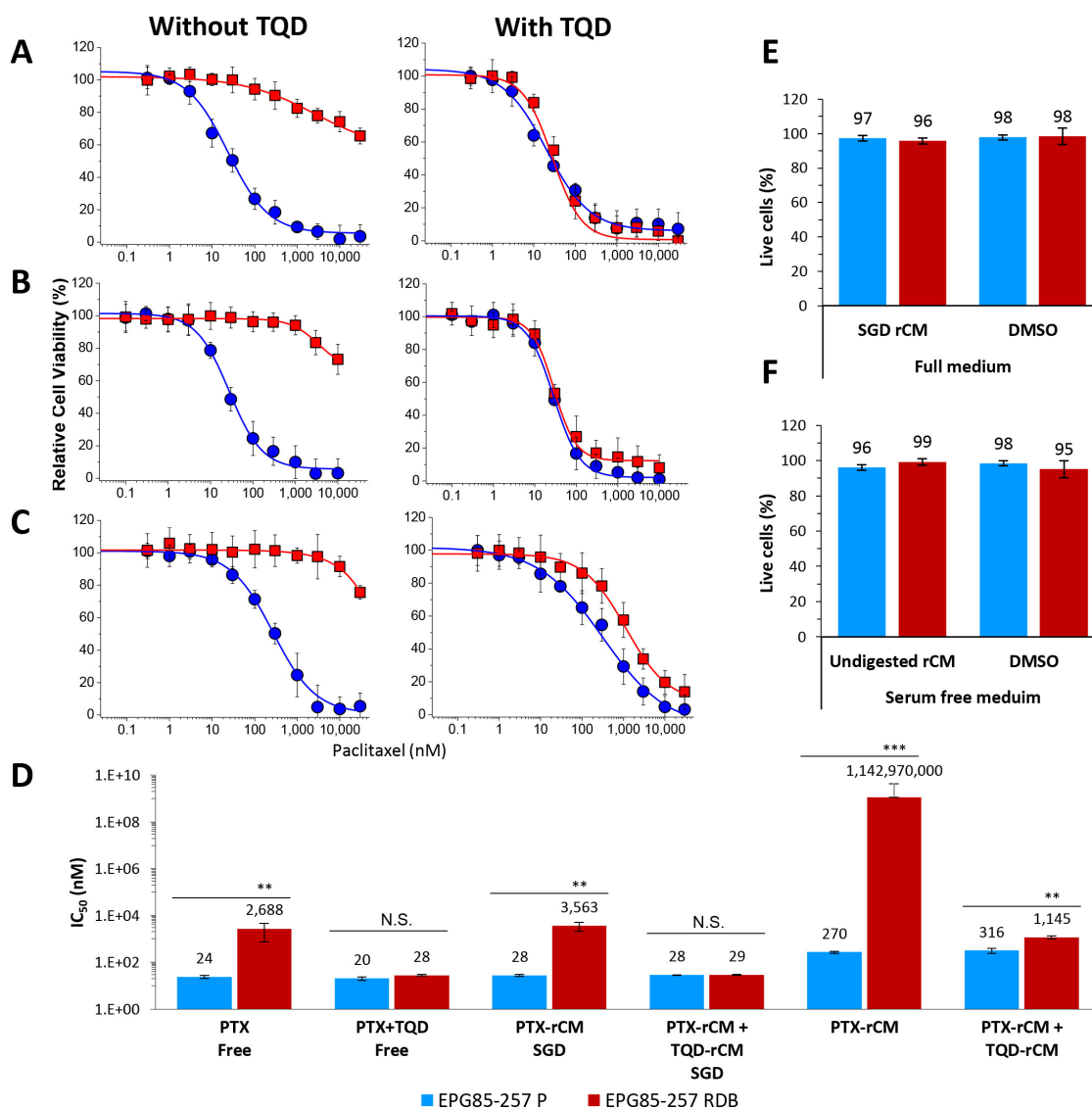


Fig. 5. Cytotoxicity assays. Relative cell viability as a function of drug concentration of: (A) free (untreated) drugs, (B) drug-rCM following SGD and (C) drug-rCM before SGD were examined using EPG85-257P, parental cell line (●) as well as EPG85-257RDB MDR subline (■) in the presence (right panel) or absence (left panel) of 0.8 μ M TQD. Values presented are means \pm SE. Lines represent sigmoidal model curve fits using Equation (2). (D) IC₅₀ values derived from the fitted dose-response curves; N.S. indicates a non-significant difference, ** indicates $P < 0.001$ and *** indicates $P < 0.0001$ as determined by student's t-test. Percentage of live cells in the control solutions: (E) digested rCM and 0.1% (v/v) DMSO in complete growth medium and (F) undigested rCM and 0.1% (v/v) DMSO in SFM.

The cytotoxic activity of the undigested, drug-loaded rCM, was determined in SFM to evaluate the efficiency of drug entrapment prior to gastric digestion. Undigested PTX-rCM exhibited significantly lower cytotoxic activity than free PTX or digested PTX-rCM, demonstrating the advantage of the encapsulated drug over the free drug for preventing premature cytotoxicity to mouth and esophagus tissues during ingestion. The IC₅₀ values were 11.4- and 9.8-fold higher for the parental cells (270 ± 27 nM) and 4.24×10^5 -fold and 3.2×10^5 -fold higher for the MDR subline ($1,143 \pm 324$ nM), respectively (Fig. 5C, D). This remarkable result confirms the high loading efficiency of the chemotherapeutic drug (i.e., there was very little unencapsulated drug, based on the higher mean IC₅₀ values of undigested PTX-loaded rCM compared to the free drugs in parental and MDR cell lines). Expectedly, the cytotoxicity of PTX-loaded

rCM with and without undigested TQD-loaded rCM towards EPG85-257P cells was not significantly different ($P = 0.1852$). Moreover, the addition of undigested TQD-rCM did not exert a complete reversal of MDR, although the IC₅₀ value was decreased by 10^6 -fold.

3.6. Freeze drying and reconstitution

Drug-loaded rCM and β -CM samples were prepared, freeze-dried and reconstituted by the addition of DDW for either an overnight incubation or for a 1 hr equilibration while stirring. We monitored the reconstitution by size distribution measurements using DLS (Fig. 6) and by quantification of their cytotoxic activity following SGD on human gastric cancer cells using an XTT assay (Fig. 7).

The volume-weighted size distributions of reconstituted rCM,

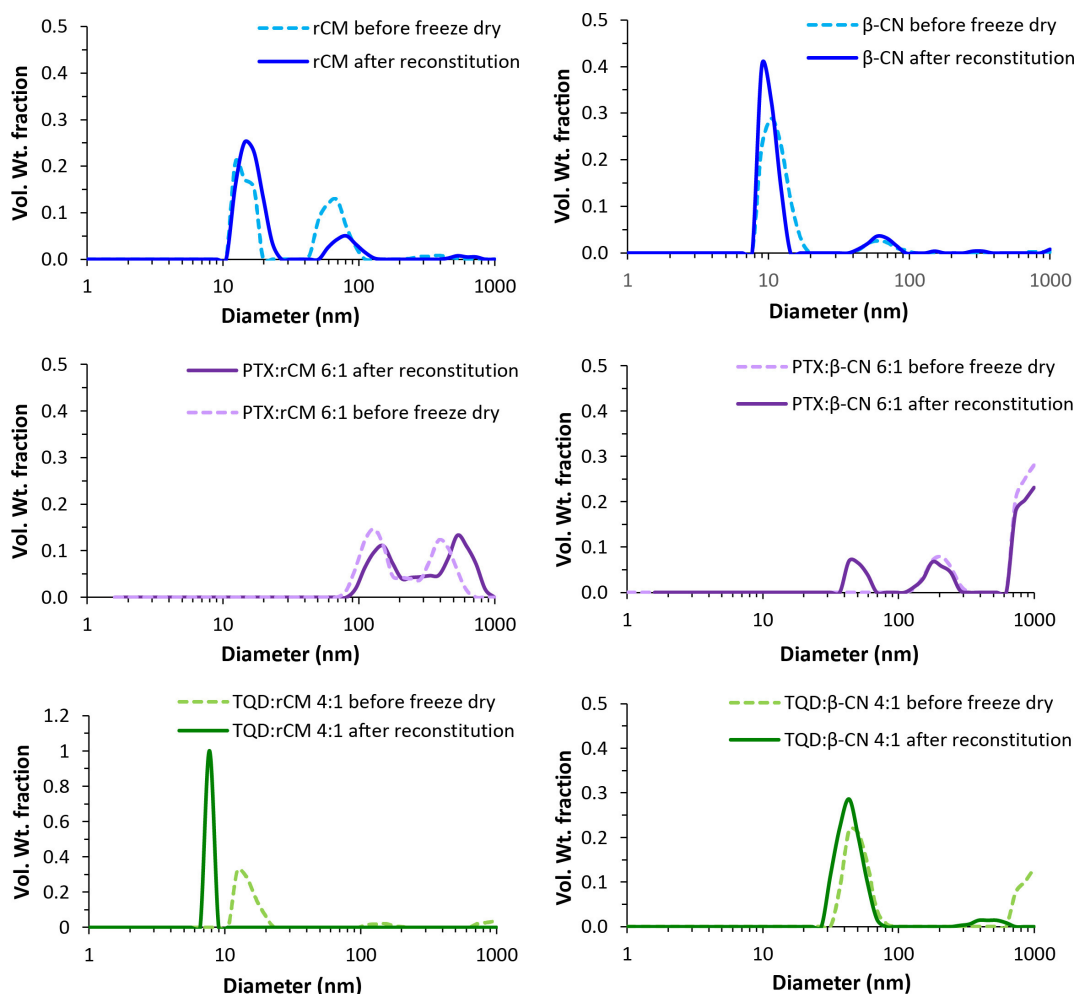


Fig. 6. Effect of freeze-drying and reconstitution on particle size distribution. Volume-weighted size distributions of rCM and β -CM with and without loaded PTX or TQD, before (dashed line) and after (solid line) freeze-drying, and reconstitution with DDW.

β -CM and drug-loaded rCM and β -CM are presented in Fig. 6. It is evident that freeze-drying and reconstitution preserved, and surprisingly, even slightly decreased the volume-weighted percentage of the larger particles fraction while increasing the smaller particles fraction in the rCM and β -CM samples. Moreover, the TQD-loaded rCM and the β -CM subpopulation peaks shifted to the left, indicating a decrease in the size of the particles. Notably, the TQD-rCM system comprised very small particles (mean sizes 55 and 7.7 nm before and after freeze drying and reconstitution respectively). As can be seen in Table 1, this process did not significantly affect the overall average size. The volume-weighted-size distribution of the β -CM and drugs loaded β -CM before freeze-drying was in line with our previously published work [25].

The cytotoxic activity of reconstituted drug-loaded rCM and β -CM was studied by an XTT assay and IC_{50} values were derived from the sigmoidal fitting of the dose-response curves using Equation (2) and are presented in Fig. 7. Freeze-dried and reconstituted samples revealed cytotoxic activities similar to those obtained for the loaded rCM (Fig. 5B, D) as well as for those of β -CM encapsulated drugs as we previously showed [25].

The size distribution and cytotoxicity results following freeze-drying and reconstitution indicate that freeze-drying and reconstitu-

tion, had only a minor positive influence of decreasing the rCM size distribution, while the cytotoxic activity of our oral nano-delivery system was retained.

Loaded Drug	Mean diameter \pm SE (nm)			
	Before freeze-drying and reconstitution		After freeze-drying and reconstitution	
	rCM	β -CM	rCM	β -CM
None	39.5 \pm 6.1	25.9 \pm 2.3	39.0 \pm 0.4	24.0 \pm 2.9
PTX	262.2 \pm 6.7	114.3 \pm 29.5	334.9 \pm 26.6	119.5 \pm 15.0
TQD	55.0 \pm 4.5	726.9 \pm 28.9	7.7 \pm 2.4	436.3 \pm 34.7

tion, had only a minor positive influence of decreasing the rCM size distribution, while the cytotoxic activity of our oral nano-delivery system was retained.

4. Discussion

Based on our previous studies [14, 16, 18, 20–25] which examined and discussed the potential of casein-based nanovehicles for oral delivery and target-activated release of a hydrophobic drug cargo in the stomach, we herein explored the rCM delivery system com-

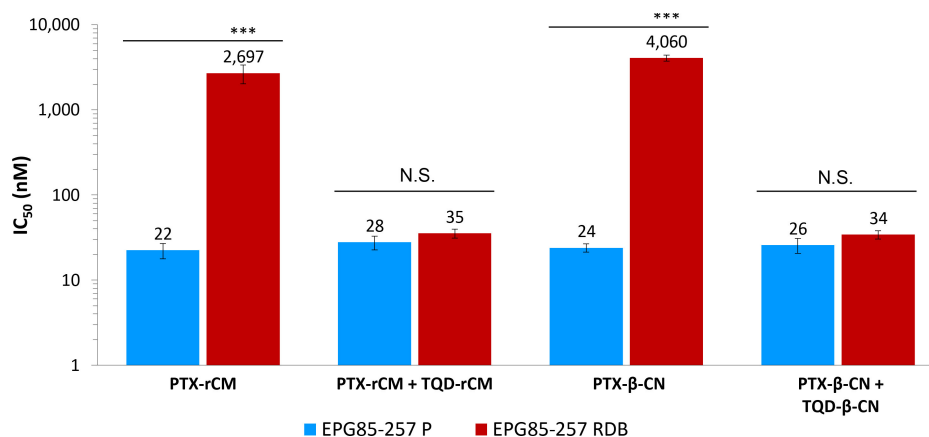


Fig. 7. The cytotoxic activity of drug-loaded rCM and β -CM after freeze-drying and reconstitution. IC_{50} values derived from the fitted dose-response curves of the relative cell viability, as a function of PTX concentration. Values presented are means \pm SE; N.S. indicates a non-significant difference, ** indicates $P < 0.001$ and *** denotes $P < 0.0001$ as determined by student's t-test.

prising two potent model drugs, each individually encapsulated. We specifically characterized rCM loaded with either a chemotherapeutic drug (PTX) or a MDR modulator (TQD) and studied the efficacy of the different systems *in vitro* before and after simulated gastric digestion, and before and after freeze-drying and reconstitution using paired human gastric carcinoma cells comprising parental cells and their P-gp-dependent MDR subline.

Our results with both PTX-rCM and TQD-rCM provide evidence for the high affinity of the drugs to the rCM, which efficiently encapsulated them. We demonstrated drug solubilization and colloidal stabilization (below the maximal loading capacity), preventing the formation of drug aggregates and crystals, using several complementary methods, including visual observation, fluorescence spectroscopy, light microscopy, and dynamic light scattering. These results were in accord with our previous studies which investigated rCM loaded with vitamin D [14, 16, 20] and docosahexaenoic acid (DHA) [18], and were similar to the results we previously reported for the same model drugs encapsulated in β -CM [21, 24, 25]. The relatively small particles formed in the TQD-rCM system suggest a low packing parameter of the TQD nanoaggregates prior to adsorption of the CN [21]. Our results regarding the binding and crystal growth prevention were also consistent with our recent study linking protein structure to its efficacy in crystal growth suppression and drug bioavailability [29]. These findings are also in agreement with other recent studies that investigated the binding of lipophilic nutraceuticals to CM, including curcumin [39, 40], β -carotene [41, 42] and EGCG [43].

As conveyed in our recent publication [25], in which we employed the same model chemotherapeutic drugs loaded within β -CM, various vehicles for oral administration of PTX have been investigated [44–48]. Moreover, recent studies examined the possibility of oral co-delivery of PTX along with a P-gp transport inhibitor [49, 50]. Nevertheless, none of these examples was designed for gastric release in a target-activated manner, as all were designed for systemic delivery of the therapeutic drug cargo.

We estimated the maximal drug loading capacity based on polarized light microscopy as well as dynamic light scattering results and found it to be at a molar ratio of 10:1 PTX:CN (356 μ g/ml), and 6:1 (162 μ g/ml) for TQD. A recent study testing transferrin-modified polyethylene glycol-phosphatidyl ethanolamine-based mi-

celles co-loaded with PTX and TQD reported a loading capacity of \sim 186 μ g/ml and \sim 459 μ g/ml, respectively [51]. Hence, the maximal loading capacities we found here for PTX and TQD encapsulated within rCM were \sim 2-fold higher and \sim 3-fold lower, respectively.

The digestive system-simulated proteolytic breakdown of rCM was fast, and within a few minutes of simulated gastric digestion, casein peptides were too small to be observed by SDS-PAGE (Fig. 4), which is consistent with the digestion of β -CN that we studied previously [24]. The rapid digestion of casein also leads to fast target-activated drug release, as we have previously shown with β -CN [24]. In both cases, 1 mg/ml casein was used. At higher concentrations, similar to those found in milk (\sim 26 mg/ml), it is expected that rCM would form a gel (curd) under acidic pH which is close to the casein isoelectric point (pI), thereby providing sustained drug release in the stomach. We have recently shown this natural gelation of rCM during a simulated digestion process [20]. Studies are underway in our lab to further characterize this gel formation effect and its influence on the release profile of the rCM payload.

Evaluation of our delivery system in a cytotoxicity assay revealed a complete reversal of P-gp-mediated MDR in EPG85-257RDB, a human MDR gastric carcinoma cell line with high P-gp overexpression. Moreover, the IC_{50} values obtained for our rCM-based delivery system following SGD were not statistically different from those obtained for the free drugs. This crucial finding confirms, as we previously reported for the β -CN-based delivery system [24, 25], that SGD treatment resulted in a complete drug release (consistent with the SDS-PAGE results which demonstrated rapid protein degradation in the gastric phase) and fully retained the pharmacological activity of these drugs. We hence demonstrated *in vitro* that the rCM-based delivery system for oral delivery and gastric target-activated release of a chemotherapeutic drug-chemosensitizer combination could overcome MDR in human gastric carcinoma cells. These results indicate that the rCM delivery system could be used to orally deliver hydrophobic drug combinations for the treatment of different types of malignant and non-malignant gastric disorders. The undigested PTX-rCM exhibited significantly lower cytotoxicity than that of the free or released drug following SGD (this observation was particularly dramatic for the MDR cells). This is an important finding for the prevention of the untoward toxicity and protection

of the upper gastrointestinal tract. Further improvement of drug loading efficiency and prevention of adverse toxicity to the buccal cavity and esophagus can be addressed by the following strategies: (a) decreasing the drug:protein molar ratio, (b) using high-pressure treatment to homogenize the system and improve drug-entrapment uniformity [14, 16, 20], (c) addition of coating layers [52, 53], and (d) protein cross-linking [25].

Freeze-drying procedures are used in the industry to enhance chemical and physical stability and to prolong shelf-life of colloidal systems [20]. We examined and compared drug-loaded rCM to drug-loaded β -CM before and after freeze-drying (with the addition of maltodextrin to the rCM as a cryoprotectant, which protects the protein from denaturation, thereby preventing aggregation of nanoparticles) and reconstitution. It is noteworthy that in both rCM- and β -CM-based delivery systems, the nanoparticle size distribution after drying and reconstitution was improved. The drug-loaded protein-based micelles retained their self-assembled structure, their cytotoxic activity and most importantly their MDR reversal capacity. These results support the further development of these casein-based oral delivery systems for therapeutic purposes to facilitate precision medicine-based drug combinations in cancer therapeutics.

In conclusion, we herein demonstrated the potential application of rCM for oral delivery and target-activated gastric release of hydrophobic drugs and their combinations. We have obtained high-affinity drug-CN binding, efficient encapsulation, high loading capacity, drug solubilization and suppression of crystallization for both PTX and TQD. Our findings provide further support for the enormous potential of casein-based nanovehicles as a novel platform for oral delivery and local target-activated release of hydrophobic drug combinations in the stomach. This delivery system could be tailored for personalizing the treatment of malignant and non-malignant gastric disorders by adapting the payload of hydrophobic therapeutic compounds required for the specific therapy. Hence, casein-based oral delivery systems provide a robust natural platform enabling a spectrum of development possibilities for gastric-activated release of synergistic drug combinations, for both local gastric treatment, and for intestinal absorption of drugs into the circulation.

Conflict of Interest

The authors declare that they have no conflict of interest related to this study.

Author Contributions

SMBZ designed the experiments; MBZ and LN performed the experiments; MBZ analyzed the data; MBZ, YDL and YGA wrote the paper; YDL and YGA supervised the project.

References

- [1] Ishigami H, Yamaguchi H, Yamashita H, Asakage M, Kitayama J. Surgery after intraperitoneal and systemic chemotherapy for gastric cancer with peritoneal metastasis or positive peritoneal cytology findings. *Gastric Cancer*, 2017; 20(1): 128–134.
- [2] Bar-Zeev M, Livney YD, Assaraf YG. Targeted Nanomedicine for Cancer Therapeutics: Towards Precision Medicine Overcoming Drug Resistance. *Drug Resist Update*, 2017; 31: 15–30.
- [3] Shapira A, Livney YD, Broxterman HJ, Assaraf YG. Nanomedicine for targeted cancer therapy: towards the overcoming of drug resistance. *Drug Resist Update*, 2011; 14(3): 150–163.
- [4] Livney YD, Assaraf YG. Rationally designed nanovehicles to overcome cancer chemoresistance. *Adv Drug Deliver Rev*, 2013; 65(13): 1716–1730.
- [5] Gottesman MM. Mechanisms of cancer drug resistance. *Annu Rev Med*, 2002; 53(1): 615–627.
- [6] Gonen N, Assaraf YG. Antifolates in cancer therapy: structure, activity and mechanisms of drug resistance. *Drug Resist Update*, 2012; 15(4): 183–210.
- [7] Raz S, Sheban D, Gonen N, Stark M, Berman B, Assaraf Y. Severe hypoxia induces complete antifolate resistance in carcinoma cells due to cell cycle arrest. *Cell Death Dis*, 2014; 5(2): e1067.
- [8] Zhitomirsky B, Assaraf YG. Lysosomes as mediators of drug resistance in cancer. *Drug Resist Update*, 2016; 24: 23–33.
- [9] Gottesman MM, Fojo T, Bates SE. Multidrug resistance in cancer: role of ATP-dependent transporters. *Nat Rev Cancer*, 2002; 2(1): 48–58.
- [10] Chen Z, Shi T, Zhang L, Zhu P, Deng M, Huang C, et al. Mammalian drug efflux transporters of the ATP binding cassette (ABC) family in multidrug resistance: A review of the past decade. *Cancer Lett*, 2016; 370(1): 153–164.
- [11] Kathawala RJ, Gupta P, Ashby CR, Chen ZS. The modulation of ABC transporter-mediated multidrug resistance in cancer: a review of the past decade. *Drug Resist Update*, 2015; 18: 1–17.
- [12] Shukla S, Ohnuma S, V Ambudkar S. Improving cancer chemotherapy with modulators of ABC drug transporters. *Curr Drug Targets*, 2011; 12(5): 621–630.
- [13] Li W, Zhang H, Assaraf YG, Zhao K, Xu X, Xie J, et al. Overcoming ABC transporter-mediated multidrug resistance: molecular mechanisms and novel therapeutic drug strategies. *Drug Resist Update*, 2016; 27: 14–29.
- [14] Semo E, Kesselman E, Danino D, Livney YD. Casein micelle as a natural nano-capsular vehicle for nutraceuticals. *Food Hydrocoll*, 2007; 21(5): 936–942.
- [15] Livney YD. Milk proteins as vehicles for bioactives. *Curr Opin Colloid Interface Sci*, 2010; 15(1): 73–83.
- [16] Haham M, Ish-Shalom S, Nodelman M, Duek I, Segal E, Kustanovich M, et al. Stability and bioavailability of vitamin D nanoencapsulated in casein micelles. *Food Funct*, 2012; 3(7): 737–744.
- [17] Głęb TK, Boratyński J. Potential of Casein as a Carrier for Biologically Active Agents. *Topics in Current Chemistry*, 2017; 375(4): 71.
- [18] Zimet P, Rosenberg D, Livney YD. Re-assembled casein micelles and casein nanoparticles as nano-vehicles for ω -3 polyunsaturated fatty acids. *Food Hydrocoll*, 2011; 25(5): 1270–1276.
- [19] Levinson Y, Ish-Shalom S, Segal E, Livney YD. Bioavailability, rheology and sensory evaluation of fat-free yogurt enriched with VD 3 encapsulated in re-assembled casein micelles. *Food Funct*, 2016; 7(3): 1477–1482.
- [20] Cohen Y, Levi M, Lesmes U, Margier M, Reboul E, Livney YD. Re-assembled casein micelles improve in vitro bioavailability of vitamin D in a Caco-2 cell model. *Food Funct*, 2017; 8: 2133–2141.
- [21] Shapira A, Assaraf YG, Epstein D, Livney YD. Beta-casein nanoparticles as an oral delivery system for chemotherapeutic drugs: impact of drug structure and properties on co-assembly. *Pharm Res*, 2010; 27(10): 2175–2186.

- [22] Shapira A, Assaraf YG, Livney YD. Beta-casein nanovehicles for oral delivery of chemotherapeutic drugs. *Nanomedicine Nanotechnology, Biol Med*, 2010; 6(1): 119–126.
- [23] Shapira A, Markman G, Assaraf YG, Livney YD. β -casein-based nanovehicles for oral delivery of chemotherapeutic drugs: drug-protein interactions and mitoxantrone loading capacity. *Nanomedicine Nanotechnology, Biol Med*, 2010; 6(4): 547–555.
- [24] Shapira A, Davidson I, Avni N, Assaraf YG, Livney YD. β -Casein nanoparticle-based oral drug delivery system for potential treatment of gastric carcinoma: Stability, target-activated release and cytotoxicity. *Eur J Pharm Biopharm*, 2012; 80(2): 298–305.
- [25] Bar-Zeev M, Assaraf YG, Livney YD. β -casein nanovehicles for oral delivery of chemotherapeutic Drug combinations overcoming P-glycoprotein-mediated multidrug resistance in human gastric cancer cells. *Oncotarget*, 2016; 7(17): 23322–23334.
- [26] Nagini S. Carcinoma of the stomach: A review of epidemiology, pathogenesis, molecular genetics and chemoprevention. *World J Gastrointest Oncol*, 2012; 4(7): 156–169.
- [27] Liu G, Franssen E, Fitch MI, Warner E. Patient preferences for oral versus intravenous palliative chemotherapy. *J Clin Oncol*, 1997; 15(1): 110–115.
- [28] Thanki K, Gangwal RP, Sangamwar AT, Jain S. Oral delivery of anti-cancer drugs: challenges and opportunities. *J Control Release*, 2013; 170(1): 15–40.
- [29] Israeli-Lev G, Pitchkhadze M, Nevo S, Fahoum L, Meyron-Holtz E, Livney YD. Harnessing proteins to control crystal size and morphology, for improved delivery performance of hydrophobic bioactives, using genistein as a model. *Food Hydrocoll*, 2017; 63: 97–107.
- [30] Portnaya I, Cogan U, Livney YD, Ramon O, Shimoni K, Rosenberg M, et al. Micellization of bovine β -casein studied by isothermal titration microcalorimetry and cryogenic transmission electron microscopy. *J Agr Food Chem*, 2006; 54(15): 5555–5561.
- [31] Rawel HM, Frey SK, Meidtnr K, Kroll J, Schweigert FJ. Determining the binding affinities of phenolic compounds to proteins by quenching of the intrinsic tryptophan fluorescence. *Mol Nutr Food Res*, 2006; 50(8): 705–713.
- [32] Shpigelman A, Israeli G, Livney YD. Thermally-induced protein-polyphenol co-assemblies: beta lactoglobulin-based nanocomplexes as protective nanovehicles for EGCG. *Food Hydrocoll*, 2010; 24(8): 735–743.
- [33] Shpigelman A, Shoham Y, Israeli-Lev G, Livney YD. β -Lactoglobulin-naringenin complexes: Nano-vehicles for the delivery of a hydrophobic nutraceutical. *Food Hydrocoll*, 2014; 40: 214–224.
- [34] Minekus M, Alming M, Alvito P, Ballance S, Bohn T, Bourlieu C, et al. A standardised static *in vitro* digestion method suitable for food—an international consensus. *Food Funct*, 2014; 5(6): 1113–1124.
- [35] Washington N, Washington C, Wilson C. Physiological pharmaceuticals: barriers to drug absorption. 2000: CRC Press.
- [36] Edelman R, Assaraf YG, Levitzky I, Shahar T, Livney YD. Hyaluronic acid-serum albumin conjugate-based nanoparticles for targeted cancer therapy. *Oncotarget*, 2017; 8(15): 24337–24353.
- [37] Benedé S, López-Expósito I, Giménez G, Grishina G, Bardina L, Sampson HA, et al. In vitro digestibility of bovine β -casein with simulated and human oral and gastrointestinal fluids. Identification and IgE-reactivity of the resultant peptides. *Food Chem*, 2014; 143: 514–521.
- [38] Ye A, Cui J, Dalgleish D, Singh H. Formation of a structured clot during the gastric digestion of milk: Impact on the rate of protein hydrolysis. *Food Hydrocoll*, 2016; 52: 478–486.
- [39] Pan K, Zhong Q, Baek SJ. Enhanced dispersibility and bioactivity of curcumin by encapsulation in casein nanocapsules. *J Agr Food Chem*, 2013; 61(25): 6036–6043.
- [40] Pan K, Luo Y, Gan Y, Baek SJ, Zhong Q. pH-driven encapsulation of curcumin in self-assembled casein nanoparticles for enhanced dispersibility and bioactivity. *Soft Matter*, 2014; 10(35): 6820–6830.
- [41] Sáiz-Abajo MJ, González-Ferrero C, Moreno-Ruiz A, Romo-Hualde A, González-Navarro CJ. Thermal protection of β -carotene in re-assembled casein micelles during different processing technologies applied in food industry. *Food Chem*, 2013; 138(2): 1581–1587.
- [42] Moeller H, Martin D, Schrader K, Hoffmann W, Lorenzen PC. Native casein micelles as nanocarriers for β -carotene: pH-and temperature-induced opening of the micellar structure. *Int J Food Sci Technol*, 2017; 52(5): 1122–1130.
- [43] Haratifar S, Meckling K, Corredig M. Antiproliferative activity of tea catechins associated with casein micelles, using HT29 colon cancer cells. *J Dairy Sci*, 2014; 97(2): 672–678.
- [44] Battogtokh G, Ko YT. Self-assembled chitosan-ceramide nanoparticle for enhanced oral delivery of paclitaxel. *Pharm Res-Dordr*, 2014; 31(11): 3019–3030.
- [45] Xu W, Fan X, Zhao Y, Li L. Cysteine modified and bile salt based micelles: Preparation and application as an oral delivery system for paclitaxel. *Colloids Surfaces B Biointerfaces*, 2015; 128: 165–171.
- [46] Joshi N, Saha R, Shanmugam T, Balakrishnan B, More P, Banerjee R. Carboxymethyl-chitosan-tethered lipid vesicles: hybrid nanoblocket for oral delivery of paclitaxel. *Biomacromolecules*, 2013; 14(7): 2272–2282.
- [47] Ahmad J, Mir SR, Kohli K, Chuttani K, Mishra AK, Panda A, et al. Solid-nanoemulsion pre-concentrate for oral delivery of paclitaxel: formulation design, biodistribution, and γ scintigraphy imaging. *Biomed Res Int*, 2014; 2014(4): 984756.
- [48] Sharma S, Verma A, Pandey G, Mittapelly N, Mishra PR. Investigating the role of Pluronic-g-Cationic polyelectrolyte as functional stabilizer for nanocrystals: Impact on Paclitaxel oral bioavailability and tumor growth. *Acta Biomater*, 2015; 26: 169–183.
- [49] Wang X, Chen Y, Dahmani FZ, Yin L, Zhou J, Yao J. Amphiphilic carboxymethyl chitosan-quercetin conjugate with P-gp inhibitory properties for oral delivery of paclitaxel. *Biomaterials*, 2014; 35(26): 7654–7665.
- [50] Patel K, Patil A, Mehta M, Gota V, Vavia P. Oral delivery of paclitaxel nanocrystal (PNC) with a dual Pgp-CYP3A4 inhibitor: preparation, characterization and antitumor activity. *Int J Pharmaceut*, 2014; 472(1): 214–223.
- [51] Zou W, Sarisozen C, Torchilin VP. The reversal of multidrug resistance in ovarian carcinoma cells by co-application of tariquidar and paclitaxel in transferrin-targeted polymeric micelles. *J Drug Target*, 2017; 25(3): 225–234.
- [52] Penalva R, Esparza I, Agüeros M, Gonzalez-Navarro CJ, Gonzalez-Ferrero C, Irache JM. Casein nanoparticles as carriers for the oral delivery of folic acid. *Food Hydrocoll*, 2015; 44: 399–406.
- [53] Huang J, Shu Q, Wang L, Wu H, Wang AY, Mao H. Layer-by-layer assembled milk protein coated magnetic nanoparticle enabled oral drug delivery with high stability in stomach and enzyme-responsive release in small intestine. *Biomaterials*, 2015; 39: 105–113.